International Journal of Solids and Structures 50 (2013) 3399–3405

Contents lists available at SciVerse ScienceDirect

International Journal of Solids and Structures

journal homepage: www.elsevier.com/locate/ijsolstr

Crack propagation under mode II dominance at stainless steel–epoxy interfaces with residual stresses and micro-scale roughness

M. Kanerva [a,*], J. Jokinen [a], E. Sarlin [b], O. Saarela [a]

[a] Aalto University, School of Engineering, Department of Applied Mechanics, P.O. Box 14300, FI-00076 Aalto, Finland
[b] Tampere University of Technology, Department of Materials Science, P.O. Box 589, FI-33101 Tampere, Finland

ARTICLE INFO

Article history:
Received 17 January 2013
Received in revised form 23 May 2013
Available online 21 June 2013

Keywords:
Interface toughness
Crack growth
Bi-material layers
Atomic force microscopy

ABSTRACT

This report describes investigations of grain boundary groove effects on mode II dominated interface fracture. The study focused on a specific interface between stainless steel and an epoxy adhesive. First, a finite element model was developed to simulate residual stresses and crack propagation. Second, the simulation results were compared with the experimental results from a previous study (Kanerva et al., 2013. Eng. Fract. Mech. 99, 147-158). Additional measurements were performed using atomic force microscopy. Based on the simulation, a 100-fold toughening effect due to the grain boundaries was determined. Implementation of flaws, in the form of interfacial voids, decreased the toughening effect by 35% and increased the mode II dominance significantly. The work underlines the practical importance of complete wetting by the adhesive and its necessary adherence to the grain boundary groove walls.

1. Introduction

The undeniable and advantageous effect of surface roughness on adhesive bonds has been known for a long time and it has been explained in terms of mechanical interlocking, the increased area of adhesion and the increased area for the diffusion of molecules on a molecular scale (Baldan, 2004). Nowadays, surface treatments can form a controlled morphology on a micrometer scale (Byskov-Nielsen et al., 2010; Kim et al., 2010). Numerical simulations could prove to be essential tools for optimising the process parameters of modern surface treatments for engineering applications (Man et al., 2005; Alfano et al., 2011) and in various medical fields (Cooper, 2000).

Zavattieri et al. and Reedy carried out fracture simulations for interfaces with a sinusoidal bond line, which basically represents a two-dimensional roughness at the interface (Zavattieri et al., 2007; Reedy, 2008). They determined a toughening effect as a function of the amplitude and wavelength of the roughness. Zavattieri et al. formulated a general interface problem in terms of stress intensity factors and, therefore, the results can be applied to a wide range of interface problems and different length-scales. Cordisco et al. reported the initiation of secondary cracks in front of the main crack in their study (Cordisco et al., 2012). Secondary cracks are important because a real interface is likely to involve flaws such as contaminants and regions of incomplete wetting that can initiate local cracks (Packham, 2003; Basu et al., 2005; Bucknall, 2007).

In contrast to the simulation of continuum interfaces, experimentations with interface fracture depend to a great degree on the length scale due to the fractal nature of real cracks and interphases (Charkaluk et al., 1998; Bouchet et al., 1999). Consequently, the determination of mechanical properties on a micro scale is challenging and data in the existing literature is scarce (Hodzic et al., 2001; Tadepalli et al., 2008). To date, there have only been a few attempts to validate the simulations of roughness on a micro scale (Towashiraporn et al., 2005; Roy et al., 2007). Even fewer studies have attempted to relate micro-scale simulations to the behaviour on a macro scale (Tvergaard and Hutchinson, 2009).

In this study, we focus on micro-scale interface fracture using a numerical simulation and experimental results. We concentrate on a specific interface between a stainless steel substrate (AISI 304, Outokumpu, Finland) and an epoxy layer (FM® 300 U, Cytec Engineered Materials). Crack propagation along the interface is simulated for a known bond line roughness, i.e., grain boundary grooves (Fig. 1(a)). Our previous studies of the interface focused on describing the micro-scale fracture processes (Kanerva et al., 2013a) and delamination on a macro scale (Kanerva et al., 2013b). Notched coating adhesion test (NCA) (Fig. 1(b)) was used for the fracture testing, in which the initiation of fracture was determined by a measured critical strain. Here, we study the effect of micro-scale roughness at the interface using the critical strain as a fitting parameter. We use atomic force microscopy to observe the fracture locus on a micro scale and to understand the behaviour of

* Corresponding author. Tel.: +358 40 718 8819.
E-mail address: Mikko.Kanerva@aalto.fi (M. Kanerva).

0020-7683/$ - see front matter © 2013 Elsevier Ltd. All rights reserved.
http://dx.doi.org/10.1016/j.ijsolstr.2013.06.008

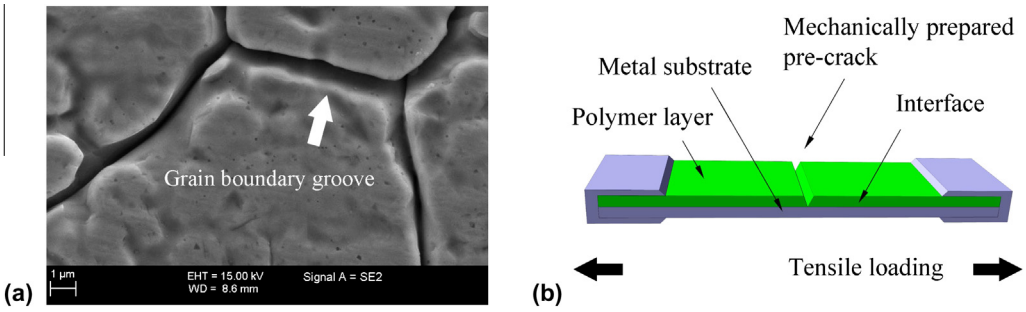

Fig. 1. Premise to the study: (a) field-emission scanning electron microscopy imaging of stainless steel surface textured by grain boundary grooves (Kanerva et al., 2013a); (b) schematic image of the NCA test setup.

the delaminating epoxy layer. Our study addresses the following issues:

1. Description of the fracture in terms of crack-tip loading mode mixity.
2. Evaluation of the toughening effect due to grain boundary grooves, in terms of a factor relating the interface fracture toughness (G_c) and the experimental, apparent fracture toughness (G_a).
3. Evaluation of the influence of flaws located at the stainless steel grain boundaries.

2. Experiments and numerical methods

2.1. Atomic force microscopy (AFM)

We used an atomic force microscope (Dimension 5000, Nanoscope 5, Veeco Instruments, USA) to study the morphology of fracture surfaces. The microscope was operated in an oscillatory mode (i.e., tapping mode) using single cantilever probes (NSC 15, 46 N/m, Micromasch, Estonia). The nominal radius of the probe's silicon tip was 10 nm and its quality was verified using a reference sample (TGT 01, Micromasch, Estonia) prior to conducting the measurements. The tip velocities (0.07–2 µm/s) were adjusted depending on the size and shape of the observed details and tip tracking. The height and phase-difference data were recorded. The samples were cut from NCA test specimens after mechanical testing and measured directly without any additional treatments.

2.2. Numerical simulation

We simulated the behaviour of an entire NCA test specimen using a two-dimensional model. We used as simple a model as possible in order to provide a high level of generality for the simulation results and to minimise the number of non-physical parameters. Sub-models were not used because of their inherent difficulties in fracture simulation (Towashiraporn et al., 2005). We studied fracture propagation at the interface between a stainless steel substrate (thickness 0.8 mm) and a polymeric epoxy adhesive layer (thickness 0.5 mm). The NCA specimen model was formed by combining two fine-meshed roughness blocks (designated R1 and R2) and two coarse-meshed tab ends. Both of the roughness blocks were 120 µm long and had one grain boundary groove each. The grooves were located in the middle of the roughness blocks at x = 60 µm and x = 180 µm. The geometry of the grain boundary grooves, which represented a realistic micro-scale roughness, was generated based on the AFM height data, as described in a previous study (Kanerva et al., 2012). Two grooves were necessary for simulating the crack propagation over a grain. In reality, the substrate surface is fully textured by the grain boundary grooves. The model is shown in Fig. 2. Primarily, we assumed linear elastic material; the constant material properties are listed in Table 1.

The simulations were performed on a finite element basis and they included two separate, subsequent calculation steps. First, a residual stress step was carried out to simulate thermal stresses. Second, a fracture step was carried out to analyse crack growth. The boundary conditions for the two steps are shown in Fig. 3. The meshing and the calculations at full (double) precision were carried out using an Abaqus® code, version 6.11/12. The element mesh consisted of linear triangle (CPS3) and linear reduced integration quadrilateral (CPS4R) plane-stress state elements (78 200 elements in total). From the modelling perspective, a crucial characteristic of AISI 304 stainless steel is that the thickness of the native oxide layer is within 5–50 Å (Lothongkum et al., 2003), i.e., it is beyond our modelling accuracy (the smallest element size in the finite element mesh). Furthermore, our modelling accuracy was assumed to be beyond the heterogeneities and non-local size effects (Nikolov et al., 2007) of the epoxy polymer.

2.2.1. Residual stress model

In reality, the modelled NCA specimen is prepared by curing the epoxy adhesive on the substrate. The cure at an elevated temperature induces residual stresses when the system is brought back to room temperature (Yu et al., 2006). Here, thermal residual stresses were simulated by presuming linear thermal expansion. The coefficient of thermal expansion (CTE) for the epoxy adhesive was based on our former study (Kanerva and Saarela, 2012), and therefore, its value specifically fits the NCA specimen deformation and cure sequence used. It should be noted that we did not aim to simulate the *formation* of stresses during the epoxy curing, but merely were interested in including the emerging stress state. The importance of residual stresses on interface fracture has been reported in the literature (e.g., Guo et al., 2006).

2.2.2. Fracture model

Crack propagation at the interface was simulated using Virtual Crack Closure Technique (VCCT). VCCT is based on the idea of a virtual crack closure, for which the required elastic strain energy is calculated and compared to a known critical strain energy release rate. A description of the VCCT method has been provided by, e.g., Krueger (2004). The force–displacement relation is linear at the crack tip when using VCCT; a fracture criterion is necessary in order to judge whether or not the crack will propagate. Here, we used a power-law criterion:

$$\left(\frac{G_I}{G_{Ic}}\right)^a + \left(\frac{G_{II}}{G_{IIc}}\right)^b = 1, \tag{1}$$

where G is the strain energy release rate, the sub index c refers to a 'critical' value and the sub-indices I and II refer to the opening and

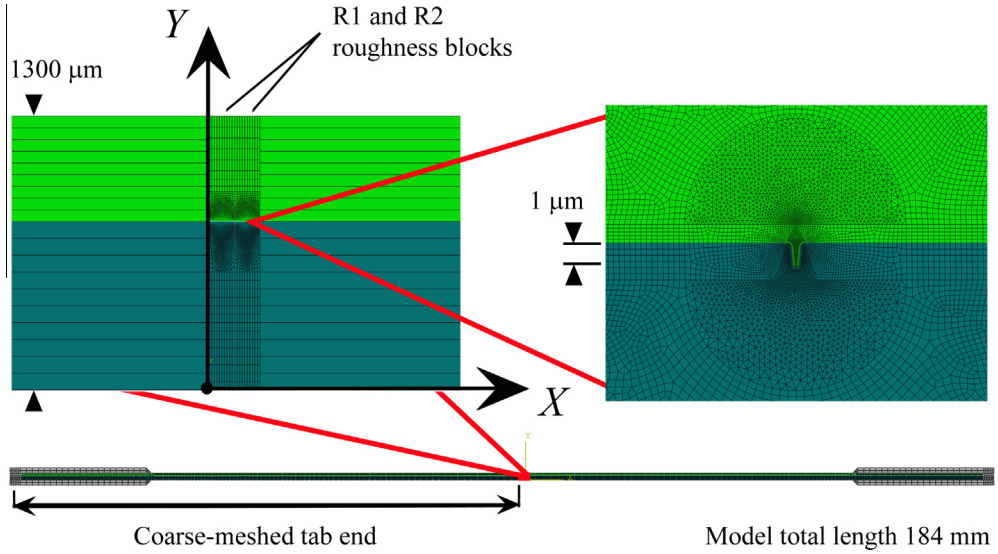

Fig. 2. Finite element model of a full-scale NCA specimen, consisting of two tab ends and two alike roughness blocks (R1 and R2). The origin of the coordinate system has been placed in the lower-left corner of the R1 roughness block. Both roughness blocks are 120 μm long in the *x*-direction and they include one grain boundary groove each. The grooves are located in the middle of the roughness blocks, at $x = 60$ μm and $x = 180$ μm.

Table 1
Constant material properties for all the simulation cases (given in model units).

Material	Young's modulus	Poisson's ratio	CTE
AISI 304	0.200 N/μm^2[a]	0.3[a]	0.000015/°C[b]
FM 300 U (epoxy)	0.0028 N/μm^2[a]	0.4[a]	0.000055/°C[a]
Gripping tabs	0.07 N/μm^2	0.3	0.000015/°C

1 N/μm^2 = 1000 GPa.
[a] Kanerva and Saarela (2012).
[b] Shiue et al. (2004).

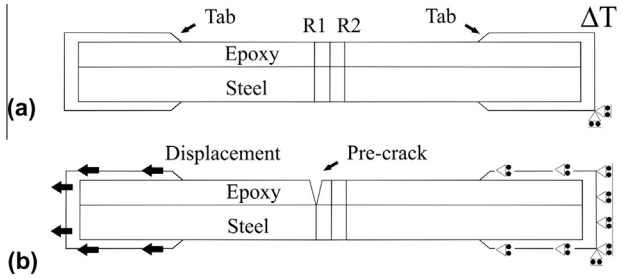

Fig. 3. Boundary conditions and load introduction for the specimen model: (a) during the residual stress simulation step and; (b) during the fracture simulation step. Figure is not in scale.

Table 2
Simulation-specific constants (given in model units).

Case designation	Thermal load, ΔT	G_{Ic}	G_{IIc}	Power law exponent
T0	0 °C	$6.4 \cdot 10^{-6}$ N/μm	$6.4 \cdot 10^{-6}$ N/μm	a = b = 1
1G	150 °C	$6.4 \cdot 10^{-6}$ N/μm	$6.4 \cdot 10^{-6}$ N/μm	a = b = 1
2G	150 °C	$6.4 \cdot 10^{-6}$ N/μm	$15 \cdot 10^{-6}$ N/μm	a = b = 1
EX	150 °C	$6.4 \cdot 10^{-6}$ N/μm	$15 \cdot 10^{-6}$ N/μm	a = b = 2

1 N/μm = 10^6 N/m.

shearing crack tip loading modes, respectively. The values of exponents *a* and *b* were typical selections for fracture simulation. The critical strain energy release rates and exponent values that we used for different simulations are shown in Table 2.

There are essentially no experimental means by which to acquire two different micro-scale G_c values. Thereby, we designated the first simulation a *reference* case (1G), where $G_{Ic} = G_{IIc}$. Likewise, we iterated a reference G_c value so that the simulated average longitudinal strain (ε_x) corresponded to the experimentally determined critical strain at the time of interface collapse, $\varepsilon_c = 0.03$ (Kanerva et al., 2013b). For this, we recorded the simulated substrate strains of the nodes representing the 50 mm gauge length of an extensometer during testing. The critical strain for an NCA specimen is defined by the level of longitudinal strain, which is high enough to drive the fracture infinitely, i.e., induce the collapse of the interface. The G_{Ic}/G_{IIc} ratio for the 2G and EX simulation cases was approximated based on the existing literature (Tenchev and Falzon, 2007).

For an actual NCA specimen, a pre-crack must be prepared mechanically using a scalpel or a wedge indentation device before the testing (Dillard et al., 1999; Kanerva et al., 2013b). The preparation of a pre-crack induces a cut through the bonded polymer layer. In our simulation, we created the pre-crack after the residual stress simulation step, by opening the contact in the epoxy layer between the R1 roughness block and the rest of the specimen (see Fig. 3(b)). Respectively, the interface crack propagation started at $x = 0$, as illustrated in Fig. 2.

2.2.3. Void model

In general, sharp roughness shapes might incur poor wetting by a high-viscosity adhesive and microscopic voids at a real substrate–adhesive interface (Packham, 2003). The grain boundary grooves on a stainless steel surface are typically very sharp, crack-like ditches (Bouquet et al., 1992) as result of harsh pickling treatments during the steel production, and it is highly probable that an adhesive would not be able to wet the sharpest ditches. Thereby, we found it important to investigate the influence of voids at the tip of the grain boundary grooves. We modelled microscopic voids by locally implementing a lack of contact along the steel–epoxy interface. The two different void configurations in our study are shown in Fig. 4. It should be noted that the local removal of contact created four additional pre-crack tips capable of propagating during the application of VCCT. The influence of the

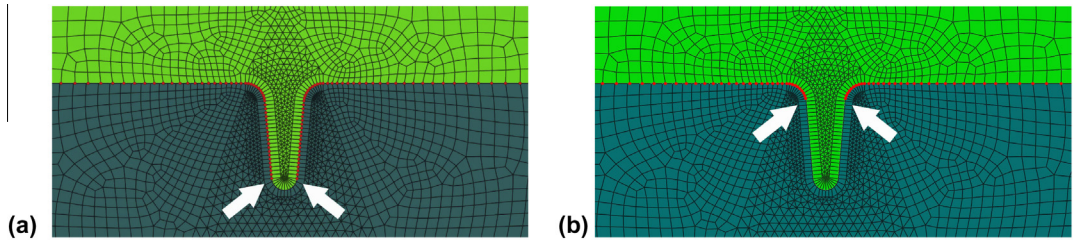

Fig. 4. Illustration of the modelled flaws at the tip of grain boundary grooves: (a) void configuration-1; (b) void configuration-2. The arrows indicate new crack propagation sites (crack tips) for the fracture simulation.

voids was studied using only the reference simulation parameters (1G), and the respective data is designated 'Voids' in the reported graphs.

3. Results

3.1. AFM measurements

Fig. 5 shows an epoxy ridge that has been pulled out from a grain boundary groove during the interface fracture. The AFM measurements confirmed that no crack had initiated into the epoxy ridge when the failure was fully interfacial. There were no significant signs of friction or sliding by the delaminated epoxy. However, the phase-difference data showed a distinct gradient at the ridge edge and could imply friction or a deviation in the failure locus on a sub-micron scale; de-adherence of stainless steel oxides is also possible. The exact geometry of a grain boundary groove varied greatly and enabled mechanical interlocking of the epoxy. This interlocking was occasionally observed as local cohesive failure of the epoxy (Fig. 5).

3.2. Simulated residual stresses and deformation

The simulated longitudinal residual stress is shown in Fig. 6. The figure shows that the simulation was in proper agreement with an experimentally validated analytical model. The simulated deformation shape was a circle arc based on a curve fit (coefficient of determination = 0.9997). The fit gave a radius of curvature of 198 cm, which corresponds well to the experimental value of 209 cm (Kanerva and Saarela, 2012).

3.3. Simulated fracture at the interface with grain boundary grooves

3.3.1. Mode mixity distribution along the rough interface

Fig. 7 shows the values of the crack-tip loading mode mixity ($\psi = \text{atan}(G_{II}/G_I)$) as a function of the location of the crack tip when the crack propagates along the stainless steel–epoxy interface. The effect of residual stresses on the mode mixity was observable only when the crack propagated along the level interface between the grooves. When a crack propagated over the both grooves, the average mode mixity for the reference simulation (1G) was $\psi = 58.7^\circ$, calculated as the arithmetic mean

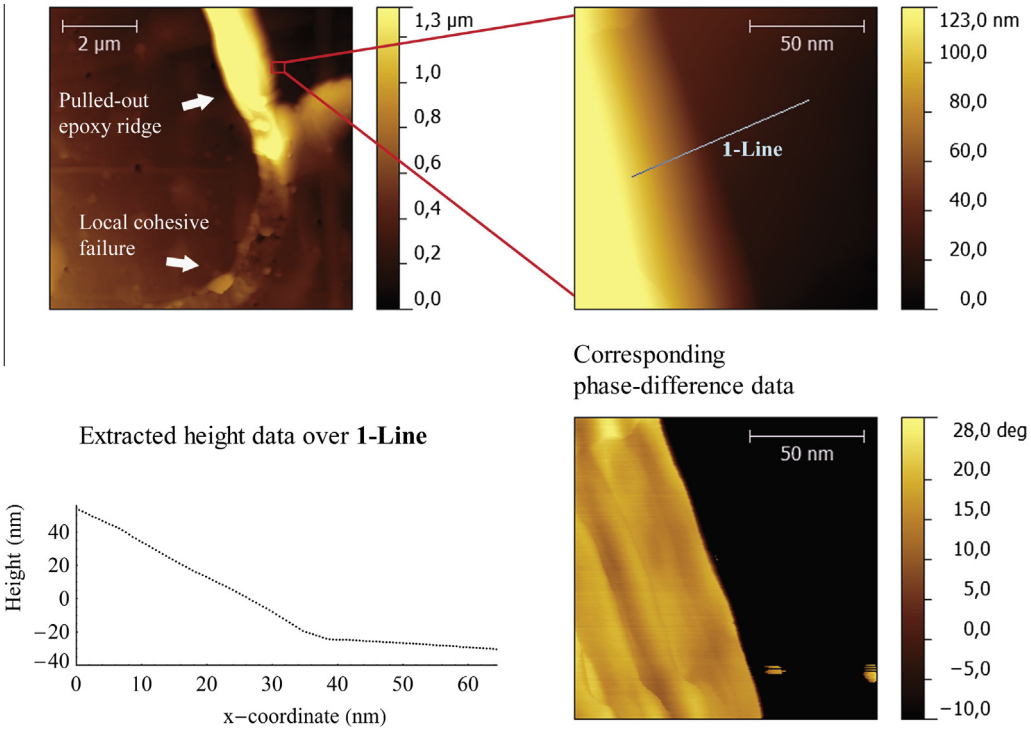

Fig. 5. Atomic force microscopy applied on the fracture surface of an NCA specimen: analysis of a pulled-out epoxy ridge. A detail analysis of the shoulder region shows no signs of nanoscale cracks, but the distinct gradient in the phase-difference image implies changes on the epoxy surface at the ridge edge. The assumed direction of crack propagation is from left to right—however, the micro-scale crack propagation might not correspond to the observed crack front on a macro scale.

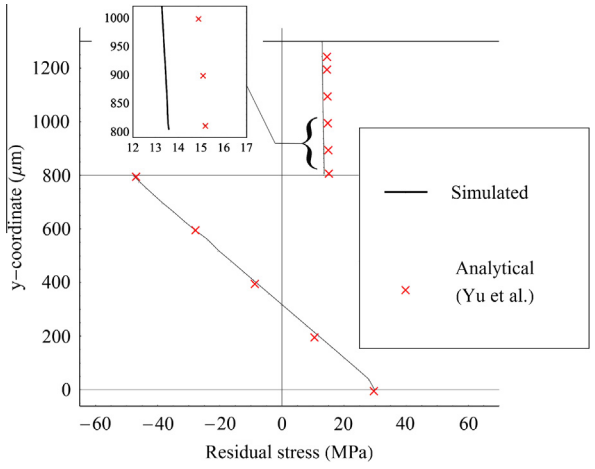

Fig. 6. Results of the residual stress simulation; longitudinal residual stress (σ_x) is plotted with an experimentally validated analytical model.

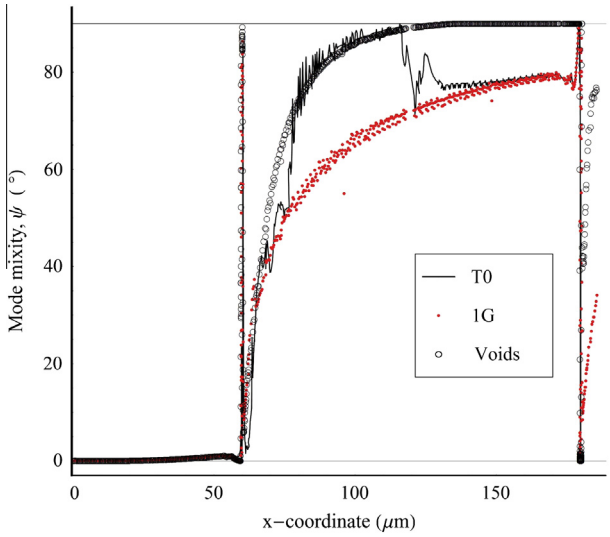

Fig. 7. Overall mode mixity as a function of crack propagation in the direction of x-axis (along the interface). Grooves are located at $x = 60$ μm and $x = 180$ μm.

over the nodes between the two groove tips. For the case in which the residual stresses were omitted (T0), the corresponding average mode mixity was $\psi = 63.9°$. These values are strongly supported by the analytical estimate based on Dundur's parameters for the bi-material interface (Suo and Hutchinson, 1990), which yields $\psi \approx 59°$ ($\alpha = -0.972$ and $\beta = -0.291$) (Kanerva et al., 2013b). When a small void was modelled at the grooves (configuration-1), a secondary crack initiated and started propagating at the latter groove. The secondary crack finally reached the main crack front at the first groove and induced a coalesced fracture. The propagation of the secondary crack occurred under intense mode II loading along the level interface because the crack was restrained from opening until the coalescence; the average mode II dominance increased by 20% ($\psi = 70.6°$) when compared to the reference simulation.

3.3.2. Mode mixity distribution along the grain boundary grooves

The mode mixity distributions exactly at the grooves represented M-shaped curves, as shown in Fig. 8. An intense mode II peak occurred at the groove shoulders. In between these two peaks, the crack tip underwent a sharp shift into mode I loading.

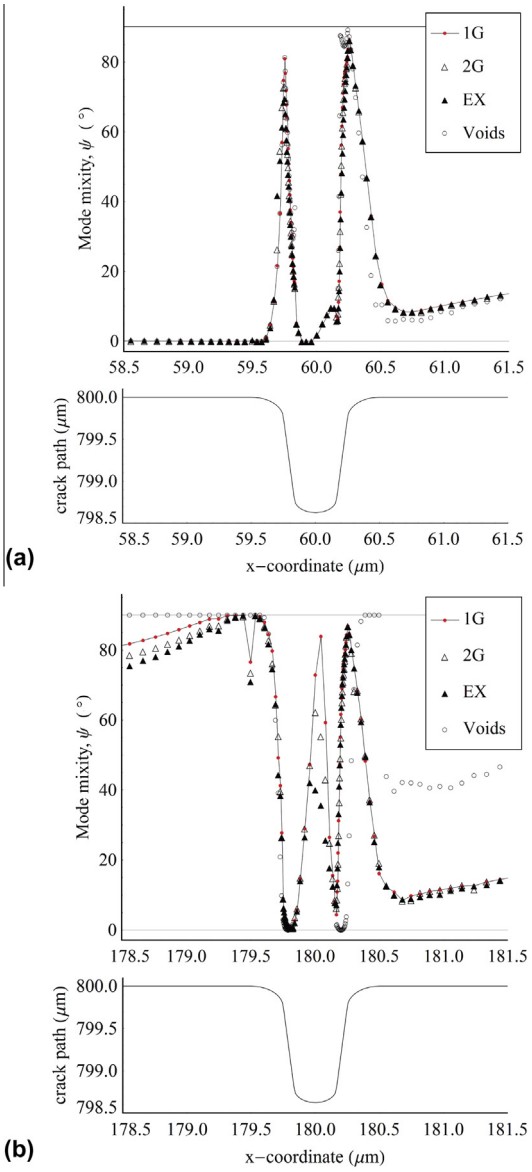

Fig. 8. Mode mixity as a function of crack propagation along the grain boundary grooves: (a) a comparison of the different fracture criteria as the crack progresses along the first groove; (b) a comparison of the different fracture criteria as the crack progresses along the latter groove. The crack path along the interface, together with the corresponding x-axis, is shown below the curves for both graphs.

It is clear that the mode II peaks at the shoulders result in a toughening mechanism, especially if there was a contact and friction between the two fresh fracture surfaces. Until progression into the first groove ($x < 59.5$ μm, Fig. 8(a)), the crack tip was loaded by opening mode I, irrespective of residual stresses. This was due to the proximity of the pre-crack, namely bending of the cut epoxy layer. There was a moderate mode II peak when a crack passed a groove tip, but this might have been related to an element mesh-dependent artefact and it did naturally not occur when voids were modelled at the grooves.

The effect of the fracture criterion was rather insignificant at the grooves. A long-lasting, mixed mode condition was only prevalent along the level interface between the two grooves; the resulting minor deviations can be observed in Fig. 8(b) when $x < 179$ μm. When the crack propagated exactly along the latter groove, the similarity of the mode mixity between the curves of different criteria was complete.

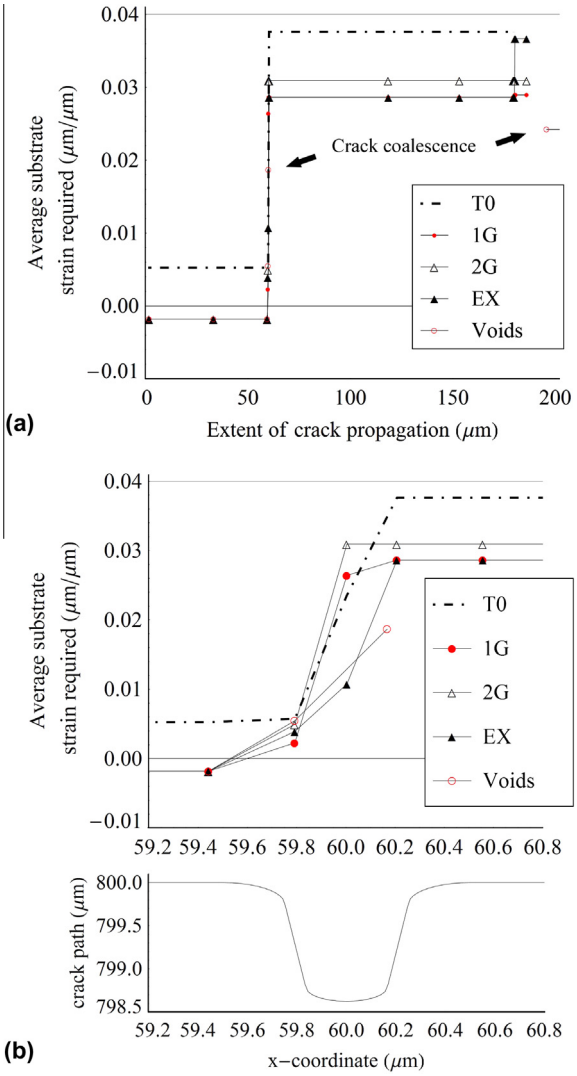

Fig. 9. The toughening effect of roughness based on the average substrate strain (ε_x) required for the crack to propagate along the interface: (a) the overall toughening effect; (b) magnification at the first groove. Note that for the 1G case with configuration-1 voids (curve: Voids) the crack propagation occurs at both grooves leading to a crack coalescence. The crack path along the interface, together with the corresponding x-axis, is shown below the curves. The experimentally determined critical strain, when the crack propagates infinitely, is $\varepsilon_c = 0.03$ (Kanerva et al., 2013b).

3.3.3. Effect of the roughness on bi-material behaviour on a macro scale

The simulated average substrate strain, which was required for the crack to propagate to a certain location, is shown in Fig. 9(a). In general, our simulations expressed unstable crack growth, which we observed experimentally for the NCA specimens, too. We observed that the simulated crack growth stalled at the first groove and that a slight increase in the strain was needed to pass the crack over to the second groove. In other words, a minimum of two grooves were needed to simulate a critical condition. The strain level was already high enough at the first groove to drive the crack infinitely only when the residual stresses were omitted (T0). The additional increase in the strain for the latter groove was highest for the simulation with the parabolic propagation criterion (EX); the parabolic criterion slightly delayed the interface collapse. For all the simulations, the toughening mostly occurred when the crack propagated upwards from the first groove, as shown in Fig. 9(b).

The decrease in the critical strain as a result of the secondary crack (applying configuration-1 voids) was 16.3% (Fig. 9(a)). Also, we iterated a new representative G_c value for the interface with the voids and arrived at 9.85 μN/μm. When the voids were extended to the walls of the grooves (configuration-2 voids), the crack front instantly propagated throughout the interface meaning, trivially that the residual stress state alone was high enough to collapse the interface.

4. Discussion

4.1. Toughening effect of the grain boundary grooves

Grain boundary grooves result in a toughening effect since a 'forced' crack path requires a higher energy release rate than what could be expected based on the critical G values in Eq. 1. That is to say, the micro-scale interface fracture toughness can be distinguished from the apparent fracture toughness on a macro scale (G_a). If the micro-scale interface fracture toughness is known, then an optimum roughness shape can be determined to gain the highest possible toughening for the material system in question.

4.1.1. Engineering toughening factor

The NCA specimen model was adjusted to behave similarly as a real test specimen in terms of critical substrate strain and when observed from the macro-scale perspective. The model utilised a micro-scale interface fracture toughness of $G_c = 6.4$ μN/μm, and an apparent fracture toughness of $G_a = 643$ μN/μm has been established during previous experiments (Kanerva et al., 2013b). A simple comparison yields an engineering toughening factor of $G_a/G_c \approx 100$. When compared to the existing literature for remote mode I loading (Cordisco et al., 2012), the determined toughening is high. Where interfacial voids were implemented, the simulation yielded a toughening factor of ≈ 65 (643 μN/μm per 9.85 μN/μm). It should be noted that we considered only the grain boundary grooves perpendicular to the direction of crack propagation.

4.2. Consideration of the micro-structure for model development

We found the use of the VCCT method and linear material to be justified based on the damage analysis carried out on the fracture surfaces, which revealed brittle fracture on a sub-micron scale (Kanerva et al., 2013a). Likewise, we simulated stainless steel as a linear material since the plastic deformation of the stiffer material at a continuum interface (between two homogenous solids) does not have a significant effect on the mode mixity and crack path (Tilbrook et al., 2005; Dillard et al., 1999). However, it is not clear how the plasticity of the stiffer (e.g., the stainless steel) or the more compliant (e.g., the epoxy) material would exactly affect the toughening effect. At a grain boundary, the yielding of the substrate is not isotropic and the micro-structure related phenomena could make a strong contribution. Specifically, individual grains can slide along one another and intra-granular dislocations prevent crack nucleation by relieving the local stresses in the metallic substrate (Qi and Krajewski, 2007; Lenci and Wolski, 2012). Moreover, a separation between two grains on a substrate surface would induce a crack at the tip of a grain boundary groove. Henceforth, our future aim is to study the influence of substrate non-homogeneity on the interface fracture.

5. Concluding remarks

A numerical model was developed to study the effects of micro-scale roughness at a bi-material interface on mode II dominated fracture. The work focused on grain boundary grooves on the sur-

face of a stainless steel substrate. The fracture was simulated using a virtual crack closure technique and thermal residual stresses were included by presuming linear thermal expansion. The simulation results were analysed in relation to fracture testing and atomic force microscopy measurements. The major conclusions of our study are as follows:

1. When a crack propagated along a grain boundary groove, the distribution of the crack-tip loading mode mixity was an M-shaped curve. For a pre-set crack path, the influence of a realistic residual stress state and the fracture criterion was negligible.
2. An engineering estimate of the toughening effect due to grain boundary grooves yielded a factor of $G_a/G_c \approx 100$. The fitted micro-scale interface fracture toughness utilised in the model was $G_c = 6.4\ \mu N/\mu m$.
3. When voids were modelled at the tip of the grain boundaries, a secondary crack occurred and the final collapse emerged in the form of a crack coalescence. Consequently, the critical strain decreased by 16% while the average mode mixity shifted from $\psi = 58.7^\circ$ to $\psi = 70.6^\circ$.

Acknowledgements

The simulation and microscopy work reported in this text were funded by the Graduate School of Aalto University's School of Engineering, Graduate School of Mechanics of Materials, and the Finnish steel industry. We are grateful to Aalto University's Nanomicroscopy Center for sharing their instruments with us and to CSC IT Center for Science for allowing us computing time.

References

Alfano, M., Lubineau, G., Furgiuele, F., Paulino, G., 2011. On the enhancement of bond toughness for al/epoxy t-peel joints with laser treated substrates. Int. J. Fract. 171, 139–150.
Baldan, A., 2004. Adhesively-bonded joints and repairs in metallic alloys, polymers and composite materials: Adhesives, adhesion theories and surface pretreatment. J. Mater. Sci. 39, 1–49.
Basu, S., Mahajan, D., Van Der Giessen, E., 2005. Micromechanics of the growth of a craze fibril in glassy polymers. Polymer 46, 7504–75018.
Bouchet, J., Roche, A., Hamelin, P., 1999. Internal stresses, young's modulus and practical adhesion of organic coatings applied onto 5754 aluminum alloy. Thin Solid Films 355, 270–276.
Bouquet, F., Cuntz, J., Coddet, C., 1992. Influence of surface treatments on the durability of stainless steel sheets bonded with epoxy. J. Adhes. Sci. Technol. 6, 233–242.
Bucknall, C., 2007. New criterion for craze initiation. Polymer 48, 1030–1041.
Byskov-Nielsen, J., Boll, J., Holm, A., Højsholt, R., Balling, P., 2010. Ultra-high-strength micro-mechanical interlocking by injection molding into laser-structured surfaces. Int. J. Adhes. Adhes. 30, 485–488.
Charkaluk, E., Bigerelle, M., Iost, A., 1998. Fractals and fracture. Eng. Fract. Mech. 61, 119–139.
Cooper, L., 2000. A role for surface topography in creating and maintaining bone at titanium endosseous implants. J. Prosthet. Dent. 84, 522–534.
Cordisco, F., Zavattieri, P., Hector Jr., L., Bower, A., 2012. Toughness of a patterned interface between two elastically dissimilar solids. Eng. Fract. Mech. 96 (192), 208.
Dillard, D., Chen, B., Chang, T., Lai, Y.H., 1999. Analysis of the notched coating adhesion test. J. Adhes. 69, 99–120.
Guo, S., Dillard, D., Nairn, J., 2006. Effect of residual stress on the energy release rate of wedge and DCB test specimens. Int. J. Adhes. Adhes. 26, 285–294.
Hodzic, A., Kim, J., Stachurski, Z., 2001. Nano-indentation and nano-scratch of polymer/glass interfaces. ii: Model of interphases in water aged composite materials. Polymer 42, 5701–5710.
Kanerva, M., Jokinen, J., Saarela, O., 2012. Interface fracture study of substrate micro-roughness using atomic force microscopy and finite element analysis. In: Interface-21 international conference on composite interfaces (Proceedings), Kyoto, Japan, August 6–8.
Kanerva, M., Saarela, O., 2012. X-ray diffraction and fracture based analysis of residual stresses in stainless steel–epoxy interfaces with electropolishing and acid etching substrate treatments. Int. J. Adhes. Adhes. 39, 60–67.
Kanerva, M., Sarlin, E., Campbell, J., Aura, K., Saarela, O., 2013a. Variation in mode ii dominated interface fracture of stainless steel–epoxy bonds. Part 2: multiscale damage analysis. Eng. Fract. Mech. 97, 244–260.
Kanerva, M., Sarlin, E., Saarela, O., 2013b. Variation in mode ii dominated interface fracture of stainless steel–epoxy bonds. part 1: Mechanical testing. Eng. Fract. Mech. 99, 147–158.
Kim, W.S., Yun, I.H., Lee, J.J., Jung, H.T., 2010. Evaluation of mechanical interlock effect on adhesion strength of polymermetal interfaces using micro-patterned surface topography. Int. J. Adhes. Adhes. 30, 408–417.
Krueger, R., 2004. Virtual crack closure technique: history, approach, and application. Appl. Mech. Rev. 57, 109–143.
Lenci, M., Wolski, K., 2012. Quantitative analysis of grain boundary sliding by atomic force microscopy for early detection of intergranular damage. Mater. Sci. Eng. A 556, 775–782.
Lothongkum, G., Chaikittisilp, S., Lothongkum, A., 2003. Xps investigation of surface films on high Cr–Ni ferritic and austenitic stainless steels. Appl. Surf. Sci. 218, 202–209.
Man, H., Zhang, S., Cheng, F., Guo, X., 2005. Laser fabrication of porous surface layer on NiTi shape memory alloy. Mater. Sci. Eng. A 404, 173–178.
Nikolov, S., Han, C.S., Raabe, D., 2007. On the origin of size effects in small-strain elasticity of solid polymers. Int. J. Solids Struct. 44, 1582–1592.
Packham, D., 2003. Surface energy, surface topography and adhesion. Int. J. Adhes. Adhes. 23, 437–448.
Qi, Y., Krajewski, P., 2007. Molecular dynamics simulations of grain boundary sliding: the effect of stress and boundary misorientation. Acta. Mater. 55, 1555–1563.
Reedy, E., 2008. Effects of patterned nanoscale interfacial roughness on interfacial toughness: a finite element analysis. J. Mater. Res. 23, 3056–3065.
Roy, S., Darque-Ceretti, E., Felder, E., Monchoix, H., 2007. Cross-sectional nanoindentation for copper adhesion characterization in blanket and patterned interconnect structures: experiments and three-dimensional FEM modeling. Int. J. Fract. 144, 21–33.
Shiue, R., Chang, C., Young, M., Tsay, L., 2004. The effect of residual thermal stresses on the fatigue crack growth of laser-surface-annealed AISI 304 stainless steel. Part i: computer simulation. Mater. Sci. Eng. A 364, 101–108.
Suo, Z., Hutchinson, J., 1990. Interface crack between two elastic layers. Int. J. Fract. 43, 1–18.
Tadepalli, R., Turner, K., Thompson, C., 2008. Effects of patterning on the interface toughness of wafer-level Cu–Cu bonds. Acta mater. 56, 438–447.
Tenchev, R., Falzon, B., 2007. Experimental and numerical study of debonding in composite adhesive joints. In: International conference on composite materials (Proceedings), Kyoto, Japan, July 8–13.
Tilbrook, M., Reimanis, I., Rozenburg, K., Hoffman, M., 2005. Effects of plastic yielding on crack propagation near ductile/brittle interfaces. Acta mater. 53, 3935–3949.
Towashiraporn, P., Subbarayan, G., Desai, C., 2005. A hybrid model for computationally efficient fatigue fracture simulations at microelectronic assembly interfaces. Int. J. Solids Struct. 42, 4468–4483.
Tvergaard, V., Hutchinson, J., 2009. Analyses of crack growth along interface of patterned wafer-level Cu–Cu bonds. Int. J. Solids Struct. 46, 3433–3440.
Yu, Y., Ashcroft, I., Swallowe, G., 2006. An experimental investigation of residual stresses in an epoxy–steel laminate. Int. J. Adhes. Adhes. 26, 511–519.
Zavattieri, P., Hector, L., Bower, A., 2007. Determination of the effective mode-i toughness of a sinusoidal interface between two elastic solids. Int. J. Fract. 145, 167–180.